Di- and trivalent Bis(stannolediides) of Dysprosium and Terbium: A novel class of High-Performance Single Molecule Magnets

Xiaofei Sun,[a] Alexander Hinz,[a] Stefanie Maier,[a] Da Jin,[a] Masaichi Saito,[b] Sören Schlittenhardt*,[c,d] Mario Ruben*[c,e,f] and Peter W. Roesky*[a,c]

[a] Institute for Inorganic Chemistry, Karlsruhe Institute of Technology, Engesserstr. 15, 76131, Karlsruhe, Germany.

[b] Department of Chemistry, Graduate School of Science and Engineering, Saitama University, Shimo-okubo, Sakura-ku, Saitama-city, Saitama 338-8570, Japan.

[c] Institute of Nanotechnology, Karlsruhe Institute of Technology (KIT), Hermann-von-Helmholtz-Platz 1, 76344 Eggenstein-Leopoldshafen, Germany.

[d] Institute of Physical and Theoretical Chemistry, Goethe University Frankfurt, Max-von-Laue-Str. 7, 60438 Frankfurt am Main, Germany.

[e] Centre Européen de Science Quantique (CESQ), Institut de Science et d'Ingénierie Supramoléculaires (ISIS, UMR 7006), CNRS-Université de Strasbourg, 8 allée Gaspard Monge BP 70028, 67083 Strasbourg Cedex, France.

[f] Institute of Quantum Materials and Technologies (IQMT), Karlsruhe Institute of Technology, Hermann-von-Helmholtz-Platz 1, 76344 Eggenstein-Leopoldshafen, Germany.

Abstract

Two isostructural homoleptic η^5-stannole complexes of trivalent lanthanides [Ln(η^5-L^{Sn})$_2$K(thf)$_4$], where Ln = Tb, Dy and L^{Sn} = [1,4-bis-(*tert*-butyl-dimethylsilyl)-2,3-bis-phenyl-stannolediide], have been synthesized via salt metathesis of the ligand's bis-potassium salt with anhydrous lanthanide iodide. The trivalent complex [Tb(η^5-L^{Sn})]$^-$ was obtained by subsequent removal of the potassium cation. In contrast, the same reaction of [Dy(η^5-L^{Sn})]$^-$ led to the divalent complex [Dy(η^5-L^{Sn})]$^{2-}$ in a unprecedent reaction pathway. These four complexes can be considered as the very first examples of homoleptic compounds with heavy atom group 14 heterocyclic ligands. Magnetic investigations reveal single molecule magnet behavior for all investigated complexes. The trivalent Dy complex is found to be a remarkable SMM with an energy barrier of 1375 K and a blocking temperature of 54 K, while the [Dy(η^5-L^{Sn})]$^{2-}$ complex is a rare example of a divalent Dy complex showing magnetic anisotropy. These results prove the potential of the homoleptic bis(stannolediides) of dysprosium and terbium as novel class of promising magnetic complexes within future molecular quantum information concepts.

Introduction

Single molecule magnets (SMMs) have potential in high-density data storage,[1] quantum information technology and spintronics.[2] Currently, the advancement of SMMs is typically based on maximizing the two key experimental parameters: the effective energy barrier (U_{eff}) to magnetic reversal and the blocking temperature (T_B) below which magnetic hysteresis can be observed. Due to the large magnetic anisotropy, lanthanide-based SMMs stand out as promising candidates to drive ground breaking advances in molecular magnetic performance.[3] Historically, the first lanthanide SMMs $[Ln(Pc)_2]^-$ (Ln = Tb, Dy, Pc = dianion of phthalocyanine) with U_{eff} values of 330.9 K (Tb) and 40.3 K (Dy) were introduced by Ishikawa and coworkers in 2003,[4] which were later integrated into devices to be read out at the single-molecule level[5] implementing quantum algorithms into a SMM.[6] In 2011, the first organometallic lanthanide SMM $[(C_5Me_5)Er(Cot)]$ was reported by Gao and exhibits an U_{eff} of 323 K.[7] The enhancement of the magnetic properties of lanthanide SMMs is closely related to their molecular architectures.[8] For Dy^{3+} and Tb^{3+} with oblate-spheroidal electron densities, axial ligand fields are predicted to enhance the U_{eff} values. Following this design strategy, the enormous potential of dysprosium complexes in this regard has been discovered recently. The magnetic anisotropy of the oblate Dy^{3+} ion can be strongly enhanced by being sandwiched between two bulky cyclopentadienides ($Cp^R = C_5R_5$) derivatives, enforcing a highly axial ligand field. A family of dysprosocenium sandwich-type cations $[Dy(Cp^R)_2]^+$ with magnetic hysteresis at up to liquid nitrogen temperature have been disclosed. The pioneering example is $[Dy(Cp^{ttt})_2]^+$ (Cp^{ttt} = $C_5H_2tBu_3$-1,2,4) reported in 2017 which exhibits magnetic hysteresis at 60 K,[9, 10] while for $[Dy(Cp^{iPr5})(Cp^*)]^+$ ($Cp^{iPr5} = C_5iPr_5$, $Cp^* = C_5Me_5$) hysteresis was observed at the current record temperature of 80 K.[11] Comparably, the bis-Cp^{ttt} Tb species $[Tb(Cp^{ttt})_2]^+$ was disclosed in 2018,[12] however, with magnetic hystereses at much lower temperatures compared to the Dy analogs.

More recently, the synthetic concept has already been extended by isolobal replacement of one C-R group by a heteroatom fragment which also allowed the synthesis of high performance Dy SMM compounds.[13, 14] To date, instances of such homoleptic Dy sandwich-type SMMs include the bis-phospholyl[15] and bis-boroledііde[16, 17] Dy cation and anion, respectively, which exhibit U_{eff} values and blocking temperatures comparable to the $[Dy(Cp^R)_2]^+$ complexes. Analogous Tb species with such Cp-type heterocyclic ligands for comparison of the magnetic properties remain elusive.

The utilization of dianionic heavy group 14 cyclopentadienides (silole,[18-21] germole,[19, 21-27] stannole[28] and plumbole[20, 29-33]) enabled potential for novel structural motifs and unique chemical bonding as they are even stronger donors than monoanionic Cp derivatives. However, at the same time, the coordination chemistry of these non-stabilized dianionic ligands poses a great synthetic challenge because of their intrinsically high reactivity and sensitivity, that has not yet been solved for dysprosium complexes. Compared to the parent Cp-type ligand, such dianions exhibit more versatile reactivity and coordination modes due to the additional lone pair at the heteroatom. This type of ligands has only been recently introduced into the coordination sphere of rare-earth metals (Fig. 1). In 2021, Tan isolated for the first time a series of yttrium germole complexes.[26] As for the homoleptic yttrium complex **I**, in addition to the η^5-coordination by two germoles, each Y metal is additionally coordinated to a neighboring germole via its η^1-mode, thus resulting a dimeric structure in the solid state. Similar dimeric structures were obtained by some of us in 2022 for the heteroleptic lanthanum sandwich compound (**II**) with silole and cyclooctatetraenide (COT).[19] When using the germole instead, a one-dimensional coordination polymer (**III**) was isolated, which still exhibits the La–Ge intermolecular interactions. Apparently, due to the lone pair of electrons, the Lewis-basic silole and germole are acting as σ-donating ligands for the rare-earth metals as well, preventing their action as solely axial ligands (π-donor) without the extra η^1-coordination (σ-donor). This has made it particularly difficult to obtain a high-performance Dy SMM with such heterocycles. One approach to overcome these challenges is to utilize the heaviest plumbole dianion, which lacks intermolecular Pb–Er interactions due to its weaker σ-donor ability. The heteroleptic COT-Er SMM **IV** with magnetic hysteresis up to 5 K was isolated by Ruben and Roesky.[31] Later on, it was shown that by combining the COT and germole dianions, the Er complexes were isolated as monomeric **V** or polymeric species **VI** without σ-coordination.[21, 27] The use of the lightest congeners, siloles, led to ring-opening of THF (**VII**) due to the strong nucleophilicity of the silicon center.[21] Avoiding THF as solvent circumvented this problem and the first silole COT complex with Er (**VIII**) was recently synthesized. The magnetic properties of all the erbium SMMs (**IV**-**VIII**) are primarily influenced by the equatorial crystal field provided by $[COT]^{2-}$ ligands, despite variations in the heteroatoms, these changes do not significantly impact the SMM properties.

Contrasting the well-known homoleptic group 13 and 15 dysprosocenium SMMs, the analogous monomeric group 14 dyprosocenium anion $[Dy(L)_2]^-$ has remained elusive due to synthetic challenges. Moreover, while compounds with Si, Ge and Pb metallole ligands have been established in the last three years, the dianionic stannole has only been utilized for

transition metals for a long time[34-39] and only very recently been incorporated in the COT-Er SMM **IX**.[40] This gap in knowledge has led us to target the synthesis of homoleptic Ln bis-stannolediide complexes, aiming to explore a new frontier in lanthanide SMM chemistry considering both the unique structure motif and promising magnetic properties.

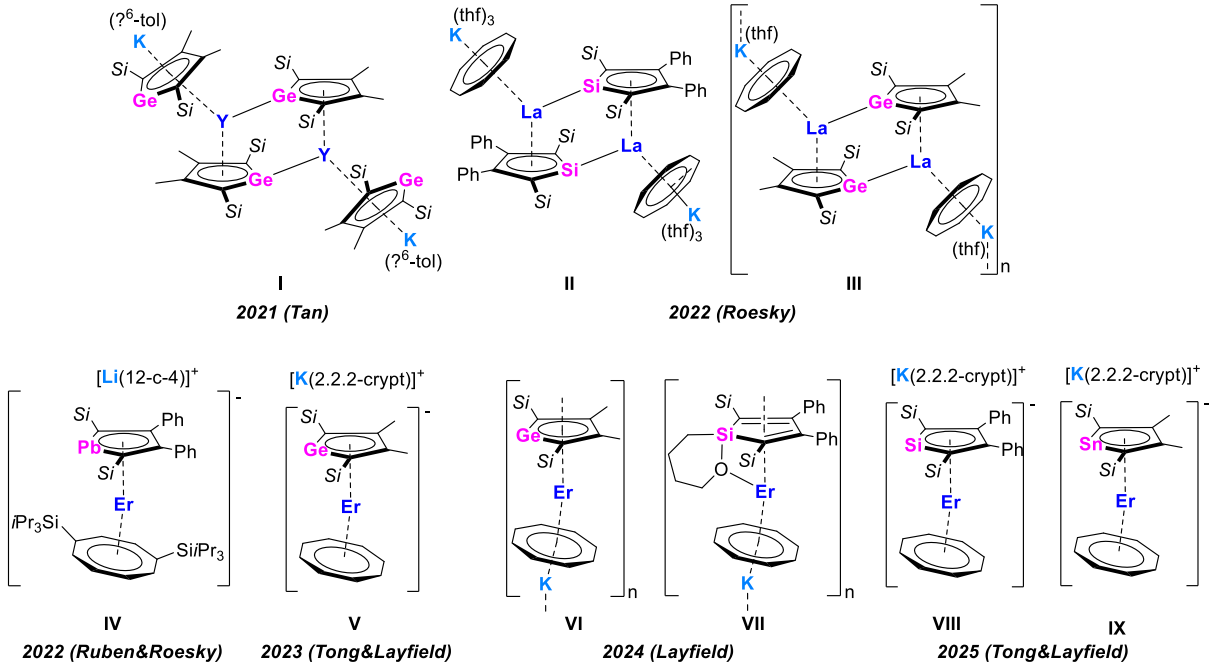

Fig. 1 Selected example of rare-earth metal compounds with dianionic heavy group 14 cyclopentadienides.[19, 21, 26, 27, 31, 40] *Si* = $SiMe_3$ in **I-III** and **V-IX**; Si = Si*t*BuMe_2 in **IV**.

Results and Discussion

The dilithium salt of the stannole $[Li_2(\eta^5\text{-}L^{Sn})]$ (L^{Sn} = [1,4-bis-(*tert*-butyl-dimethylsilyl)-2,3-bis-phenyl-stannolediide]) was previously reported by Saito.[28, 41] However, attempts to perform salt metathesis reactions of the dilithiostannole with the dysprosium (pseudo)trihalides proved unsuccessful. The increased lattice energy of potassium (pseudo)halides was identified as potential solution to this problem. Consequently, the dipotassium salt of the stannole was prepared straightforwardly by reduction of the 1,1,3,4-tetraphenyl-2,5-bis-(*tert*-butyl-dimethylsilyl)-stannole[41] with an excess amount of elemental potassium (Fig. 2a). Upon reduction, the color of the solution changed from yellow to dark brown. After filtration and evaporation of all volatiles, $[K_2(Et_2O)_{0.45}(\eta^5\text{-}L^{Sn})]$ (**1**) was obtained in 69% yield and was used for the following reactions without further purification. The dipotassiostannolediide **1** was characterized by multinuclear NMR spectroscopy and single crystal X-ray diffraction (SCXRD) analysis. Single crystals of **1** were obtained from a THF/*n*-hexane mixture and the solid-state structure consists of a one-dimensional coordination polymer where each stannole

ring is η^5-coordinated by two K cations (Fig. 2b). Additionally, one of the two K cations is η^1-coordinated to the Sn lone pair of the neighboring stannole ring, thus forming polymer chain. The ring planarity (sum of inner angles: 540.0°) and the similar C–C bond lengths within the SnC_4 ring hints at the aromatic nature of the stannole dianion, and these bonding metrics are comparable to those of its lithium derivative.[41] The ^{119}Sn NMR spectrum reveals a singlet at 615 ppm, which is shifted to higher frequencies in comparison to its dilithium analog (473 ppm).[41]

The bis-stannolediide lanthanide compounds [Ln(η^5-L^{Sn})$_2$K(thf)$_4$] (**2-Ln**, Ln = Tb, Dy) were synthesized *via* salt metathesis from anhydrous LnI_3 (Ln = Tb, Dy) and [$K_2(Et_2O)_{0.45}(\eta^5$-$L^{Sn})$] in 1:2 molar ratio in THF (Fig. 2c). After stirring the reaction mixture at room temperature for 16 h, the insoluble metathesis salt (KI) was filtered and the remaining THF solution was concentrated and layered with *n*-pentane. Dark red block-shaped crystals were obtained after two weeks, the mother liquid was decanted, and the crystals were dried under vacuum for 30 min, giving an overall yield of 47% for **2-Dy** and 57% for **2-Tb**, respectively. Single crystal X-ray diffraction analysis revealed the formation of the bis-stannolediide complexes, in which the potassium cation is η^1-coordinated to the Sn lone pairs of both stannolediide rings (Fig. 2d, e). To complete the coordination sphere, four additional THF molecules are coordinated to the K ion. Both complexes are isostructural and crystallized in the monoclinic space group *C*2 with half of the molecule in the asymmetric unit, with the Ln···K located at the crystallographic *C*2 axis. The Ln···K distance of 5.3223(13) Å (**2-Dy**) and 5.3427(8) Å (**2-Tb**) are too long to represent any bonding interaction. As expected, the Ln ion is coordinated to the two stannole rings in η^5-mode and the torsion angle between the two stannole rings is about 31.0° in both complexes (Fig. 2d, e). The distance between the Ln and the centroid of the stannole ring is 2.3039 Å for **2-Dy** and 2.3232 Å for **2-Tb**. This difference is expected, as the Tb^{3+} ion is slightly larger than the Dy^{3+} ion. The lanthanide–centroid distance in **2-Dy** is even shorter than the respective distances in the bis-phospholide complex (2.354(3) Å)[15] and [Dy(Cp^{ttt})$_2$]$^+$ (2.316(3) Å) but well-comparable to the values in other Dy metallocenium ions (2.244(6)–2.340(7)°). The lanthanide–centroid distance in **2-Tb** is almost the same as in the terbocenium cation [Tb(Cp^{ttt})$_2$]$^+$ (2.325(4) Å)[12] but slightly shorter than in [Tb(Cp^{iPr5})$_2$]$^+$ (2.356(6) Å).[42] This highlights the strong electronic influence of the dianionic stannole ring in axial positions, as despite the anticipated increase of the Ln–ligand distance due to steric bulk, the stannole is located in close proximity to the metal ion. The anionic [Ln(η^5-L^{Sn})$_2$]$^-$ motif is slightly bent with Ct–Ln–Ct angle of 154.3° for Dy and 153.5° for Tb. These values lie in the range of previously reported metallocene-type Dy and Tb cations. For example, the bis(stannolediide)

compounds **2-Ln** are slightly more linear than the Ln cations $[Dy(Cp^{ttt})_2]^+$ (152.845(2)°),[9, 10] $[Tb(Cp^{ttt})_2]^+$ (152.2(2)°) and $[Dy(Cp^{iPr4})_2]^+$ (147.2(8)°)[43] but more bent compared to the bis-phospholide Dy cation (157.94(4)°)[15] and the bis-boroledііde Dy anions (156.5°, 158.6(3)°, 161.4(3)°).[16, 17]

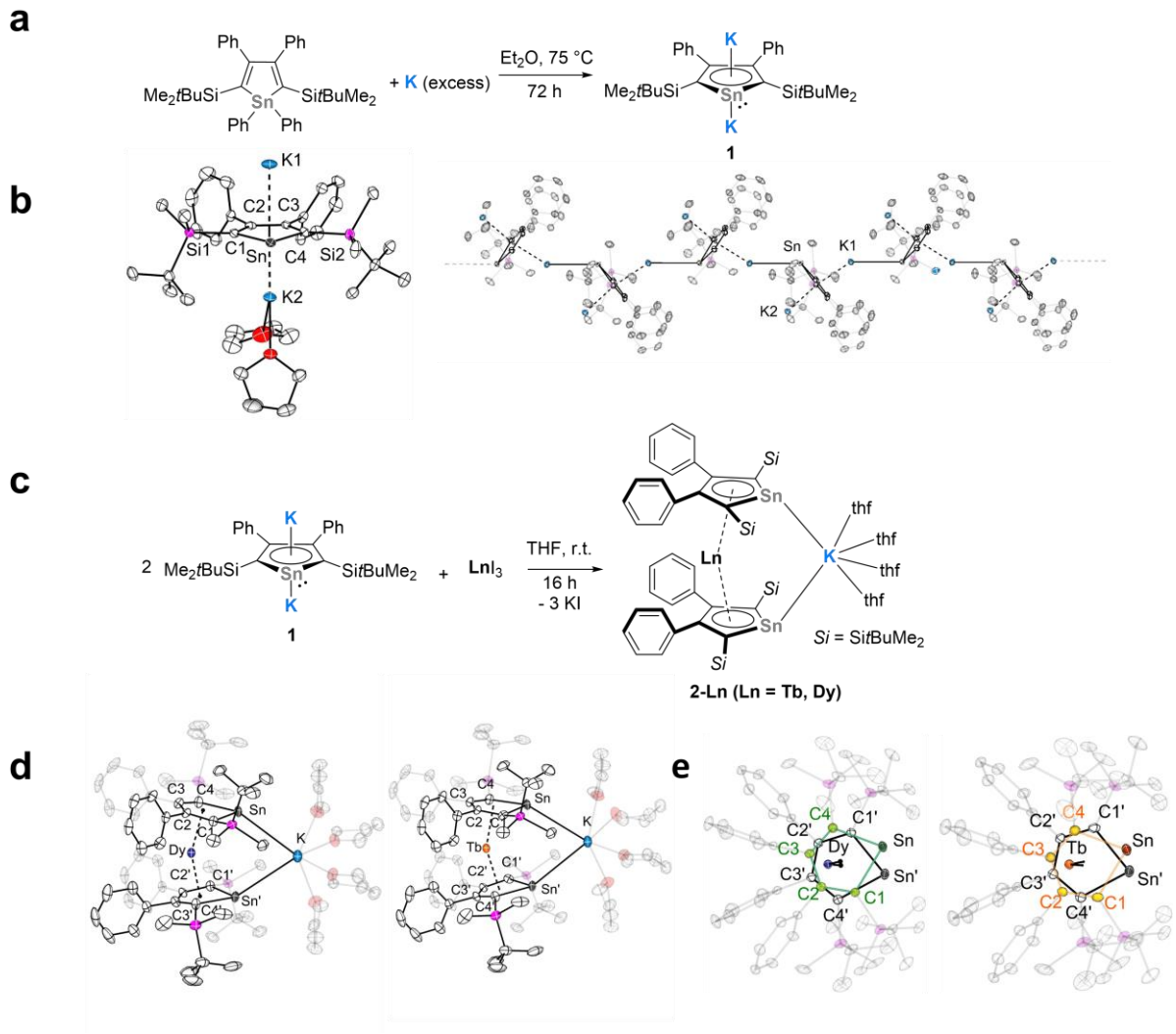

Fig 2. Synthesis of the dipotassium salt of stannole 1 and the bis(stannoldiide) complexes 2-Ln (Ln = Dy and Tb). a. Synthesis of **1** by reduction of 1,1,3,4-tetraphenyl-2,5-bis-(*tert*-butyl-dimethylsilyl)-stannole with potassium. **b.** The asymmetric unit of the coordination polymer of complex **1** (left) and a section of the polymeric chain of **1** (right). **c.** Synthesis of **2-Ln** (Ln = Dy and Tb) by reaction of **1** with LnI_3. **d.** Molecular structures of complexes **2-Dy** (left) and **2-Tb** (right) in the solid state. **e.** Top view of complexes **2-Ln**. The $[K(thf)_4]^+$ fragment is omitted for clarity. All compounds are shown with 50% probability thermal ellipsoids. All hydrogen atoms are omitted for clarity. Selected bond distances and angles are summarized in the ESI.

The reactions of the K-bridged Tb(III) and Dy(III) complexes **2-Ln** with 18-crown-6 allowed the abstraction of the K^+ ion and enabled the formation of the respective anionic sandwich complexes **3-Tb** and **4-Dy** (Fig. 3a). SCXRD analysis revealed that the molecular structures of

3-Tb and **4-Dy** are charge-separated ion pairs. In the case of the Tb compound **3-Tb**, red single crystals were formed from a concentrated benzene solution. The molecular structure of **3-Tb** features the expected monoanionic homoleptic Tb(III) sandwich compound (Fig. 3b). The cationic part consists of a crown ether-solvated potassium cation, which is connected to the next K^+ unit via a bridging 18-c-6 molecule. In the anionic sandwich part, upon decoordination of the bridging K cation, the Ct1–Tb–Ct2 angle of 155.295(4)° becomes slightly more linear and the Tb–Ct distances (Tb–Ct1 2.3432, Tb–Ct2 2.3391) become slightly longer in comparison to the structural metrics in **2-Tb**. For Dy, an unexpected redox event occurred, which resulted in the formation of the dianionic Dy(II) sandwich complex **4-Dy**. Single crystals of **4-Dy** were formed from a solvent mixture of THF and benzene. The dianionic sandwich structure of **4-Dy** is depicted in Fig. 3c. The Dy atom in located on the center of inversion, which gave a Ct–Dy–Ct' angle of 180.0° and a C_{2h} symmetry in first proximity. This perfectly linear coordination geometry of the divalent Dy species is very rare for a $4f^n$ lanthanide metallocene, since in most cased bending motifs are obtained as trivalent compounds **2-Ln** and **3-Tb** This difference between the divalent compound **4-Dy** and the trivalent compounds **2-Ln** and **3-Tb** is consistent with the geometries of the $[(Cp^{iPr5})_2Dy]$ (180°)[42] and $[(Cp^{iPr5})_2Dy]^+$ (162°).[43] The distance between the Dy atom and the ring centroid of the stannole rings is 2.3034(1) Å, which is almost unchanged in comparison to the value in **2-Dy**.

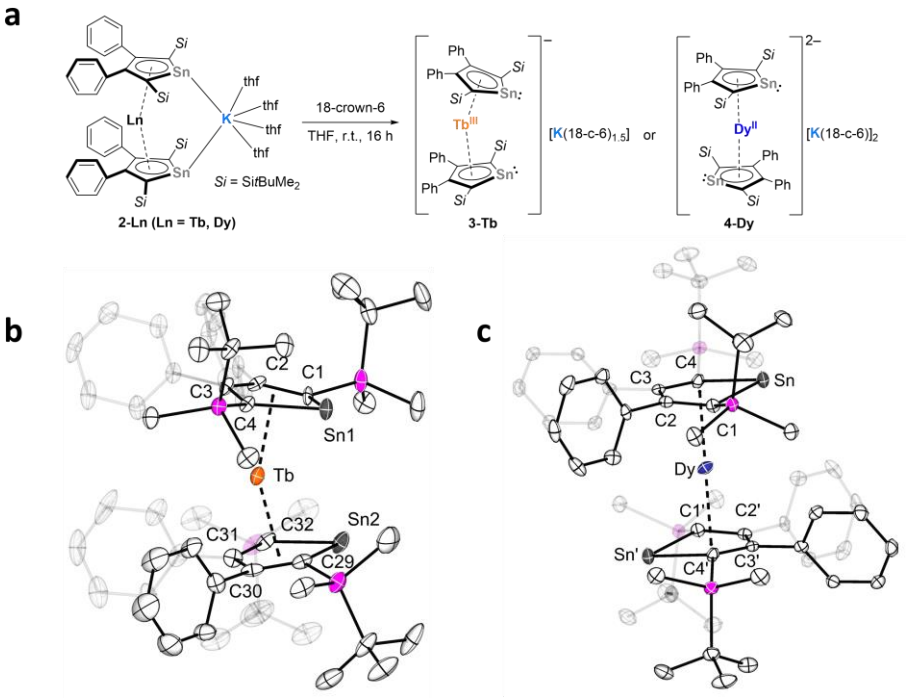

Fig 3. Synthesis of the Tb(III) complex 3-Tb and the Dy(II) complex 4-Dy. a. Synthesis of **3-Tb** and **4-Tb** by reaction of **2-Ln** with 18-crown-6. **b.** Molecular structure of complexes **3-Tb. c.** Molecular structure of complexes **4-Dy.** All compounds are shown with 50% probability

thermal ellipsoids. All hydrogen atoms are omitted for clarity. Selected bond distances and angles are summarized in the ESI.

As the main driving force of the described synthesis was the exploration of the resulting magnetic properties of the Ln-sandwich complexes, we performed SQUID-magnetometric analyses on compounds **2-Ln** (Ln = Tb, Dy), **3-Tb** and **4-Dy**. Based on previously reported systems and theoretical models of SMM performance, we expected to find complexes with relatively high U_{eff} and T_B. Starting with the Tb(III) analogues **2-Tb** and **3-Tb**, applying an external magnetic field of 1000 Oe (0.1 T), we have observed room temperature values of the molar susceptibility temperature product χT of 12.48 and 11.07 cm^3 K mol^{-1}, respectively (Fig. S12, S14). For both samples, the values are within approximately 6 % deviation from the theoretical value of a single Tb(III) ion with J = 6 and g_J = 3/2 of 11.82 cm^3 K mol^{-1}. Such deviations can be ascribed to the preparation procedure, where slightly inaccurate determination of the sample mass in the glovebox can introduce error of a few percent very quickly. Upon cooling the samples down, χT decreases very slowly while above 100 K and starts decreasing more rapidly below that temperature. Interestingly, for **2-Tb** the data below 100 K reveals a sort of plateau around 50 K followed by a sudden very strong drop below 10 K. On the other hand, **3-Tb** shows a rather constant decrease in the temperature range of 100 K – 2 K. Additionally to the data recorded upon cooling, we have investigated the T-dependent susceptibilities of both samples upon heating in a field-cooled (FC) and zero-field-cooled (ZFC) scan (Fig. S12, S14). For both compounds the ZFC and FC data deviate from the cooling data below 90 K. The ZFC and FC curves of **2-Tb** remain on top of each other below 90 K until they separate around 15 K. This separation can be interpreted as a hint of magnetic blocking at this temperature. Both curves have an intense, sharp maximum at approximately 11 K (FC) and 12 K (ZFC). For **3-Tb**, both ZFC and FC data show a broad maximum around 50 K. In the T range from 90 K – 30 K, the susceptibility values are very comparable between the FC and ZFC measurements while they deviate below 30 K (Fig. S12, S14). It should be noted that the splitting between ZFC and FC data is much less pronounced than in **2-Tb**.

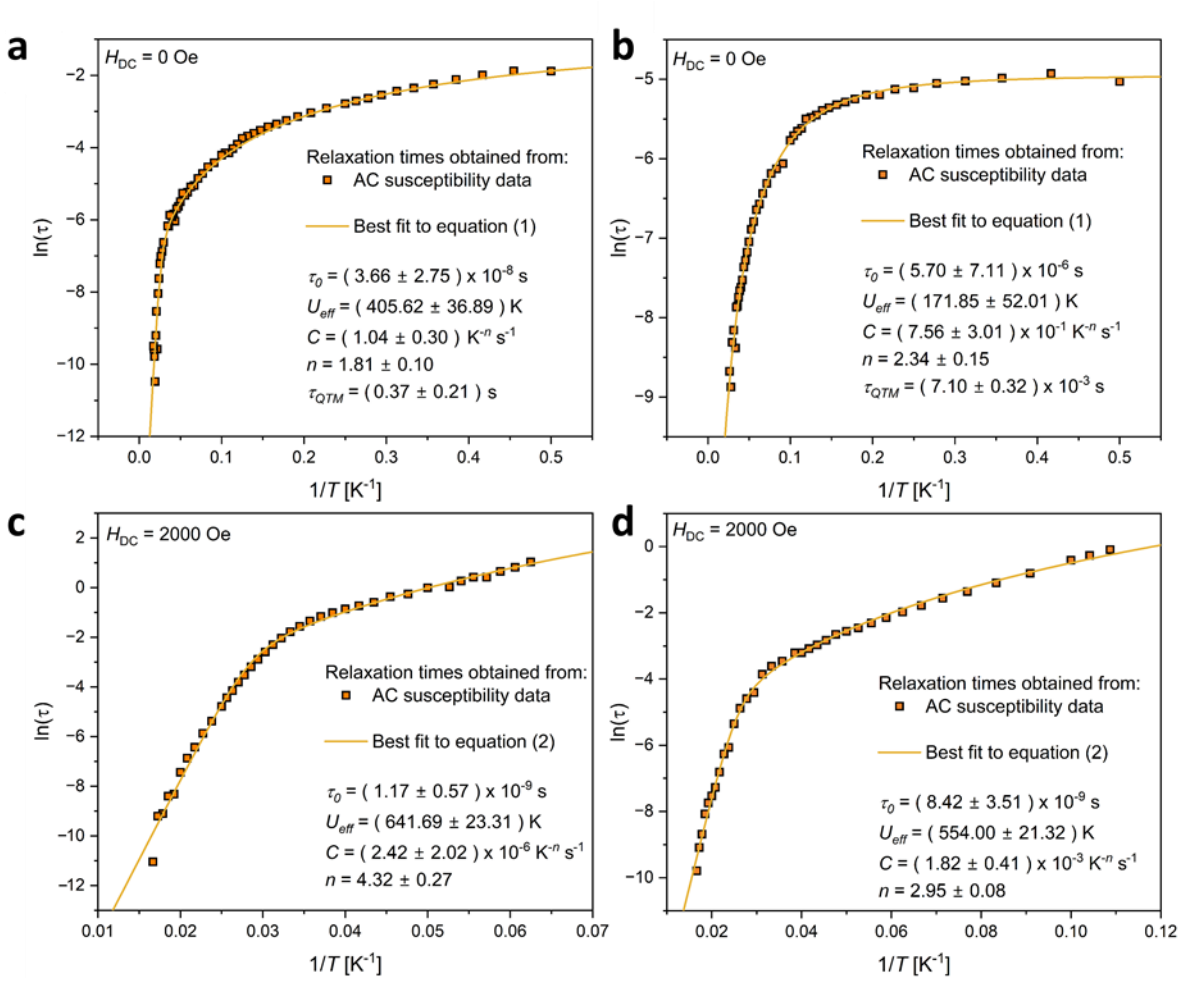

Fig. 4. Temperature dependent relaxation times for the two Tb(III) complexes. **a. 2-Tb**, recorded without an external field. **b. 3-Tb**, recorded without an external field. **c. 2-Tb**, recorded under the application of 2 kOe. **d. 3-Tb**, recorded under the application of 2 kOe.

While temperature dependent susceptibility data can provide an idea about the magnetic relaxation behavior, dynamic AC susceptibility measurements allow a much greater insight. Therefore, frequency and temperature dependent AC susceptibility measurements on **2-Tb** and **3-Tb** were performed. At the lowest available temperature of 2 K and without the application of an external field, a maximum in the out-of-phase component of the susceptibility of **2-Tb** is observed around 1 Hz (Fig. S25). The maximum decreases in intensity upon increasing the temperature, which is commonly observed for SMMs, unless strong antiferromagnetic interactions are present between paramagnetic centers.[44] Additionally, with increasing temperature the maximum shifts first slowly later quickly to higher frequencies. Such behavior is typical for dominant Raman relaxation at lower temperatures and Orbach relaxation, which is becoming dominant at elevated temperatures. The highest temperature at which reliable data were acquired was 58 K. It should be stated here, that at low *T* a rather high out-of-phase signal is obtained at high frequencies, which might be related to a fast-relaxing species, possibly

introduced by partial decomposition of the sample. While the position of the maximum doesn't remain identical at low *T*, which would be a sign of relaxation via QTM, tunnelling is still likely to be present and relevant at low *T*. Thus, we have performed similar AC susceptibility measurements under the application of an external DC magnetic field of 2000 Oe which, by lifting the degeneracy of the ground state, should improve the energy barrier to relaxation. The field was chosen as the field resulting in the slowest relaxation (maximum observed at lowest frequency). Under the applied field, the lowest temperature at which a maximum is observed shifted to 16 K, where the maximum is centered around 0.1 Hz and the signal remains observable up to 60 K (Fig. S32). The trend at which the maximum is shifting its frequency position resembles that of Raman and Orbach relaxation. Analogously, AC susceptibility measurements at zero field and 2000 Oe were performed on a sample of **3-Tb**. At zero field and 2 K a maximum is observed around 30 Hz, therefore, significantly faster compared to **2-Tb** (Fig. S46). A reliable maximum was detected up to 38 K. The *T*-dependence of the maximum suggests much stronger contribution of quantum tunnelling compared to **2-Tb**, as the maximum doesn't shift in frequency at low *T*. Similarly, the available temperature range was improved by the application of the external 2000 Oe field, resulting in an observed maximum between 9 K and 60 K (Fig. S53). In order to validate out assumptions, the recorded frequency dependent in-phase and out-of-phase components were simultaneously fit to a generalized Debye model allowing the determination of the relaxation time τ (Table S2, S3, S5, S6). Based on the description above, we have attempted fits of τ vs. *T* using a combination of Orbach, Raman and QTM processes for the data collected at zero external field using equation (1):

$$\tau^{-1} = {\tau_0}^{-1} \exp{}^{-U_{eff}}\!\Big/_{k_B T} + C\,T^n + {\tau_{QTM}}^{-1} \quad (1)$$

A very good fit was obtained for **2-Tb** yielding the parameters τ_0 = 3.66 x 10^{-8} s, U_{eff} = 406 K (282 cm^{-1}), *C* = 1.04 K^{-n} s^{-1}, *n* = 1.81 and τ_{QTM} = 0.37 s (Fig. 4a). Similarly, a good fit was achieved for **3-Tb** with the following parameters: τ_0 = 5.70 x 10^{-6} s, U_{eff} = 172 K (119 cm^{-1}), *C* = 7.56 x 10^{-1} K^{-n} s^{-1}, *n* = 2.34 and τ_{QTM} = 7.10 x 10^{-3} s (Fig. 4b). As the application of the external field is used to suppress quantum tunnelling of the magnetization, the data obtained from measuring at 2000 Oe were fit using equation (2) which corresponds to a combination of only Orbach and Raman type relaxation.

$$\tau^{-1} = {\tau_0}^{-1} \exp{}^{-U_{eff}}\!\Big/_{k_B T} + C\,T^n \quad (2)$$

In both cases **2-Tb** and **3-Tb** equation (2) was sufficient to produce good fits of our experimental data (Fig. 4c, d). The best fit parameters obtained were τ_0 = 1.17 x 10^{-9} s, U_{eff} =

642 K (446 cm^{-1}), C = 2.42 x 10^{-6} K^{-n} s^{-1}, n = 4.32 for **2-Tb** and τ_0 = 8.42 x 10^{-9} s, U_{eff} = 554 K (385 cm^{-1}), C = 1.82 x 10^{-3} K^{-n} s^{-1}, n = 2.95 for **3-Tb**, respectively.

Considering only Orbach relaxation, the blocking temperatures T_B of the complexes were determined when τ = 100 s, giving 18.67 K (ZF) and 25.49 K (2 kOe) for **2-Tb** and 10.30 K (ZF) and 23.88 K (2kOe) for **3-Tb**. Usually, the magnetic blocking of a molecular system is also associated with open hysteresis loops below its blocking temperature. We have performed hysteresis measurements at a field sweep rate of 50 Oe/s (Fig. S17, S22). Both systems **2-Tb** and **3-Tb** show open butterfly-like hysteresis loops at 2 K that are closed at zero field due to fast QTM. With increasing T, the opening of the loops vanishes at around 10 K and 6 K for **2-Tb** and **3-Tb**, respectively. It should be noted here that the open hysteresis loops do not match with the T_B values determined through AC magnetometry. Such behavior has also been observed for several representatives of the $Tb(Pc)_2$ family, where despite U_{eff} values above 400 cm^{-1} hysteresis has only been observed at very low T.[45] However, the trend of **2-Tb** showing better performance than **3-Tb** remains. Often changes of the magnetic properties can be correlated to structural changes of the molecular geometry. Between **2-Tb** and **3-Tb** the K cation in **2-Tb** promotes closer proximity of the two axial stannole rings: 2.3232 Å in **2-Tb** compared to 2.3432 Å and 2.3391 Å in **3-Tb**. Further, the bending angle Ct-Tb-Ct is affected by the potassium ion as well, resulting in a stronger bending of **2-Tb** (153.5°) compared to **3-Tb** (155.3°). However, the structural changes alone appear comparably small to cause a difference of the energy barriers of more than a factor of two. We believe that the potassium ion also significantly changes the electronic structure of within the aromatic stannole system, resulting in the strong performance difference between **2-Tb** and **3-Tb**.

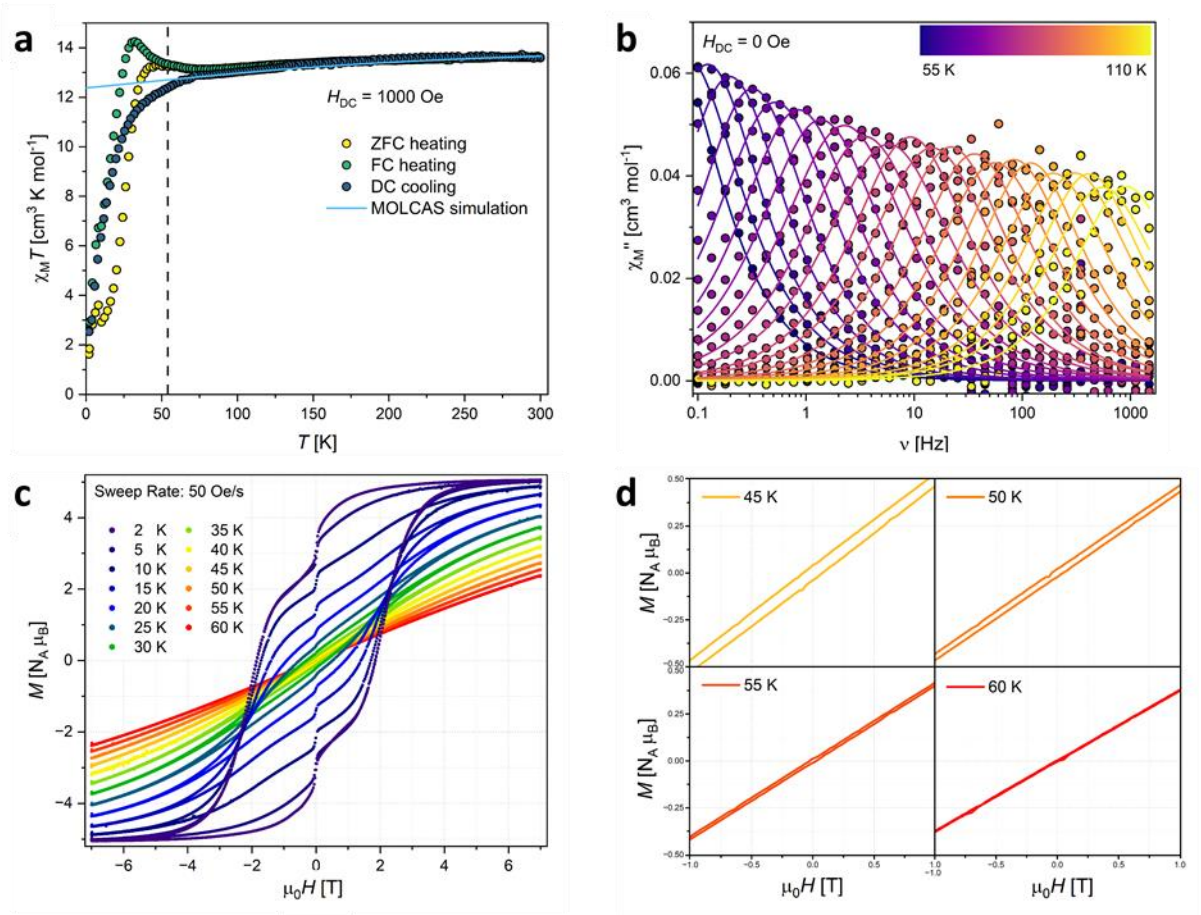

Fig. 5. a. *T*-dependence of the magnetic susceptibility of **2-Dy**. The dashed vertical line is drawn at the blocking temperature 54.05 K determined though AC susceptibility measurements as explained in the text. **b.** Frequency dependency of the out-of-phase component of the magnetic susceptibility recorded between 55 K and 110 K for **2-Dy**. The solid lines are the best fits to a generalized Debye model. **c.** Hysteresis loops measured at different *T* for **2-Dy**. **d.** Zoom in of the hysteresis loops recorded between 45 K and 60 K. At 55 K a slight opening can still be observed while the loops at 60 K can be considered fully closed.

In SMM research and especially lanthanide based SMM research, Dy(III) has been the frontrunner in terms of high performance. This is due to Dy(III)'s nature of being a Kramers ion (half integer spin) which yields a degeneracy of the m_J states of opposite sign irrespective of the environment along with strong single-ion anisotropy. The temperature dependence of the magnetic susceptibility of **2-Dy** was investigated under application of an external field of 1000 Oe (Fig. 5a). At room temperature we found a χT value of 13.61 cm^3 K mol^{-1} which is in reasonably good agreement to the expected value of 14.17 cm^3 K mol^{-1} of a single Dy(III) ion with J = 15/2 and g_J = 4/3. Upon cooling the behavior of **2-Dy** is very similar to that of **3-Tb** where χT only decreases slowly down to about 90 K after which it starts decreasing more rapidly. A plateau as it was observed for **2-Tb** is not found for **2-Dy**. Susceptibility measurements were also performed upon heating after zero-field and field cooling. Above approximately 80 K, the obtained χT values are practically identical for heating and cooling. Below 80 K, the ZFC and

FC curves are higher than the cooling data and more importantly the ZFC and FC deviate of each other below approximately 55 K, a sign of magnetic blocking. At zero field we have investigated **2-Dy** by means of AC susceptibility measurements, as shown in Fig. 5b. A reliable signal in the out-of-phase component was observed in the temperature range from 55 K to 110 K, during which the maximum shifts from the lowest observable frequency 0.1 Hz to the highest of 1500 Hz. The position shifts rather evenly across the full *T* range suggesting pure Orbach relaxation within this region. In order to have a full view of the relaxation dynamics, we have also performed time dependent magnetization decay measurements at temperatures between 2 K and 30 K. The relaxation times were obtained following the approach described by Blackmore et al,[46] for a more detailed description see SI. The combined τ vs. *T* data have been fit using equation (1). The best fit yielded the parameters: τ_0 = 9.05 x 10^{-10} s, U_{eff} = 1375 K (955 cm^{-1}), *C* = 1.17 x 10^{-9} K^{-n} s^{-1}, *n* = 4.90 and τ_{QTM} = 325.69 s. Deriving the blocking temperature T_B with τ = 100 s, gives a blocking temperature of 54.05 K, which is in perfect agreement to the observed trend in the *T*-dependent ZFC and FC susceptibilities (Fig. 5a). Hysteresis measurements with 50 Oe/s reveal a vastly open loop at 2 K, with a coercive field of 1.86 T. Around zero field a noticeable drop is observed due to quantum tunneling within that field range. The hysteresis loops are closing at temperatures between 50 K and 60 K; while at 55 K the loop can arguably still be considered open, the loops have fully closed at 60 K (Fig. 5c, d). Similar to the ZFC-FC behavior, the closing of the hysteresis loops is in very good agreement to the blocking temperature determined via AC and magnetization decay measurements. While the measured energy barrier and blocking temperature are not a new record in SMM performance, the values are still remarkable and are among the highest observed in SMM research. To the best of our knowledge, **2-Tb**, **3** and **2-Dy** are also the first examples of trivalent, homoleptic complexes of group 14 heterocycles. In comparison, the homoleptic Dy(III) based SMMs of the group 13 boron heterocyclic ligands $[(TPhBN)_2Dy]^-$ (where TPhBN = 1-piperidino-2,3,4,5-tetraphenylborolyl) reported in 2022[16] and $[Dy(BC_4Ph_5)_2]^-$ reported in 2023[17] both showed higher energy barriers of 2302 K/ 1871 K and 2159 K (the two energy barriers for $[(TPhBN)_2Dy]^-$ were determined as separate values for two disordered components of the complex) and blocking temperatures of 67 K/ 60 K and 65 K, respectively. Further, the phosphorus-containing homoleptic complex $[Dy(Dtp)_2]^+$ (where Dtp = 2,5-Ditertbutyl-3,4-dimethylpospholyl) revealed a U_{eff} value of 1760 K,[15] about 400 K higher than that of **2-Dy**, however with a considerably lower blocking temperature of 23 K. Previous reports of sandwich type Dy(III) SMMs have shown that the main geometrical factors are the metal-ring distance, usually given as the distance towards the centroid of the ring , as well as the bending angle Ct-

Dy-Ct. Interestingly, the observed Dy-Ct distance in **2-Dy** is between those observed for the two boron-containing complexes mentioned. The bending angle in **2-Dy** with 154.3° is slightly smaller, meaning the molecule is more strongly bent, compared to the two boron and phosphorus compounds which showed 161.4°, 158.6°, 156.5° and 157.9°, respectively. It should be noted, that **2-Dy** significantly differs from the referenced complexes as there is the additional bridging unit of the potassium cation. The K^+ might influence the electronic structure of the heterocyclic ligand enough, as mentioned for the Tb(III) complexes **2-Tb** and **3-Tb**, so that a direct comparison of distances and angles might not be directly applicable**.**

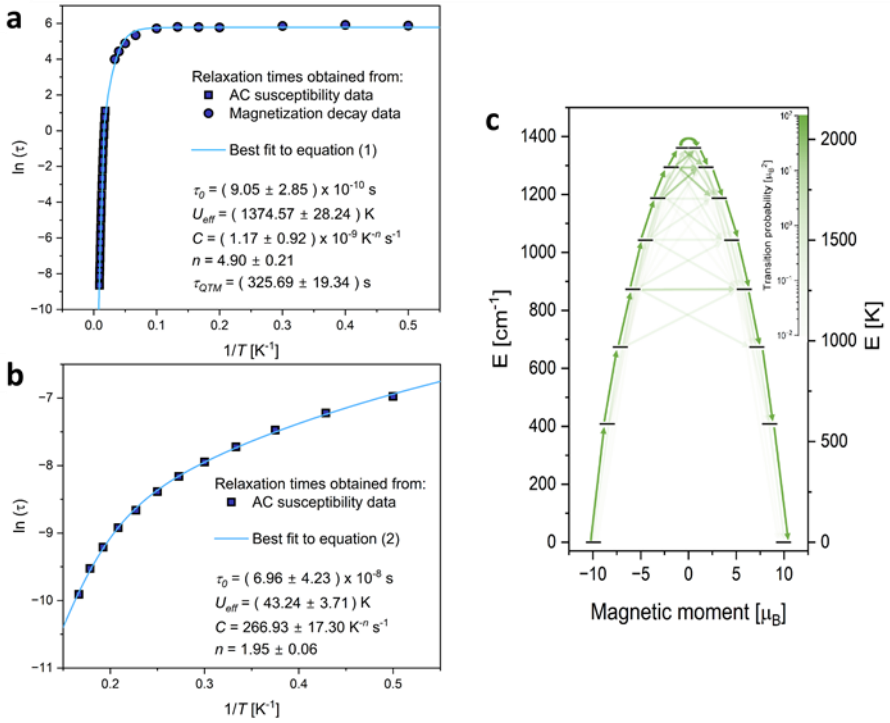

Fig. 6. a. Temperature dependent relaxation times for the two Dy complexes **2-Dy** collected without an external field and **b. 4-Dy** (bottom left) under the application of 900 Oe. **c.** Calculated energy diagram and transition probabilities between the different m_J states for **2-Dy** using the CASSCF/RASSI/SINGLE_ANISO routine.

In order to further validate the relaxation behavior of **2-Dy**, we have performed ab initio calculation using OpenMolcas[47] following the CASSCF/RASSI/SINGLE_ANISO routine on the molecular structure obtained via X-ray crystallography (for further details see SI). As expected from the experimental data, the wavefunctions of the lowest lying energy levels resemble relatively pure m_J states without much admixing (Table S8). The obtained energy diagram of the J = 15/2 multiplet is shown in Fig. 6a and c, along with calculated transition probabilities. As usually observed, without much admixing the highest transition probabilities are found for transitions of $\Delta m_J = \pm 1$. The transition probability within the third excited Kramers doublet, however, is three orders of magnitude higher than the transition probabilities

within the first and second excited doublet states. We, therefore, believe that the main relaxation pathway at elevated temperatures follows the idea of thermally assisted quantum tunneling (TA-QTM) via the third excited doublet state. The calculated energy of this state at the given level of theory is 1256.03 K (872.94 cm^{-1}) which is in decent agreement with the experimentally observed barrier of 1375 K (955 cm^{-1}).

As previously mentioned, the potassium cation in **2-Dy** makes it difficult to fully assess the structural changes in comparison to other reported homoleptic Dy(III) heterocyclic compounds which do not contain such a bridging unit. We had, therefore, attempted to remove the K^+ ion using 18-crown-6, similar to the synthesis of **3-Tb**. However, we observed the formation of the divalent species **4-Dy** which is found to be a perfectly straight sandwich complex (Ct-Dy-Ct = 180°). It is noteworthy that the reports of divalent dysprosium compounds are rather scarce. However, a structurally very comparable Dy(II) metallocene complex has been reported by Gould et al in 2019.[42] The complex $[Dy(Cp^{iPr5})_2]$ showed a similar formation of a perfectly straight geometry compared to the bent Dy(III) precursor. We have investigated the *T*-dependent susceptibility of **4-Dy** upon cooling the sample in an external field of 1000 Oe. The obtained room temperature χT value was 10.95 cm^3 K mol^{-1}, which is surprisingly low compared to the theoretical values of either 14.07 cm^3 K mol^{-1} (Dy^{II}, assuming $4f^{10}$ $5d^0$) or 17.01 / 14.51 cm^3 K mol^{-1} (Dy^{II}, assuming $4f^9$ $5d^1$ and applying an L-S or j-j coupling scheme).[42] Performing AC susceptibility measurements of **4-Dy** without the application of an external field did not give any signal in the out-of-phase component. Only under the application of an external field a frequency-dependent maximum could be observed. Under the optimal field of 900 Oe, a signal was reliably detectable in the temperature range of 2 K – 6 K, during which it shifts from approximately 200 Hz to 1500 Hz (Fig. S60). Due to the application of the external field QTM is suppressed, *vide supra*, and the temperature dependent relaxation times were fitted with Orbach and Raman relaxation using equation (2) (Fig. 6b). The obtained best fit parameters were τ_0 = 6.96 x 10^{-8} s, U_{eff} = 43 K (30 cm^{-1}), C = 266.93 K^{-n} s^{-1}, n = 1.95. The dramatic change of the relaxation behavior between **2-Dy** and **4-Dy** is caused by the Kramers and non-Kramers nature of the trivalent and divalent Dy ions. One of the main reasons Dy(III) has been the most prominent candidate in high performance SMMs is its half-integer spin, leading to the formation of degenerate Kramers doublets in the energy spectrum irrespective of the coordination environment of the ion. Upon addition of an electron in Dy(II) the Kramers character is lost and the usual approach of designing high performance SMMs is no longer applicable. It should be noted that in the mixed valence compound $[(Cp^{iPr5})_2Dy_2I_3]$ an additional electron facilitates the exchange between two Dy ions leading to huge magnetic hysteresis even at relatively high

temperatures.[48] However, the electron in this case is not located at the Dy and the magnetism is not arising from a Dy(II) species. The previously mentioned complex [Dy(Cp^{iPr5})$_2$] was reported with an energy barrier U_{eff} of 37.4 cm^{-1},[42] very comparable to our observation for **4-Dy**.

Conclusion

The trivalent and divalent lanthanide complexes reported are, to date, the first homoleptic η^5-stannole containing complexes of lanthanides and they are amongst only a few other examples of homoleptic lanthanide complexes using heterocyclic ligands. Most likely the close contact of the potassium cation alters the electronic structure of the stannole ligand in **2-Tb** in a way that is positive for its SMM performance. This might be an interesting approach to future synthesis, fine-tuning the magnetic properties of lanthanide complexes. The trivalent Dy complex **2-Dy** is found to be a zero-field SMM with a high effective energy barrier of 1375 K and a high blocking temperature of 54.05 K. It is among of the best performing SMMs to date.

Upon the removal of the bridging potassium cation from **2-Ln**, we have obtained different results for Ln = Tb(III) and Ln = Dy(III). For Tb, the treatment with 18-crown-6 resulted in the expected formation of an anionic sandwich complex **3-Tb**, with the counter cation separated from the complex. The accompanying structural changes of the Tb-Ct distances and Ct-Tb-Ct angles appear too small for the drastic change we observed in the complexes' magnetic behavior. Other than in the Tb case, for Dy attempts for a simple removal of the K^+ cation using 18-crown-6 resulted in an unprecedented reduction reaction of Dy(III) to Dy(II). Due to the intrinsic properties of Dy(II), the resulting complex **4-Dy** is a field-induced SMM with a comparably lower barrier of 43 K. Nonetheless, complex **4-Dy** is one of very few examples reported to date of an SMM based on divalent Dy.

The obtained results prove definitely the potential of the novel class of homoleptic bis(stannoldiides) of dysprosium and terbium in view of modern molecular quantum information applications.

References

1. Mannini, M. et al. Magnetic memory of a single-molecule quantum magnet wired to a gold surface. *Nat. Mater.* **8**, 194-197 (2009).
2. Bogani, L. & Wernsdorfer, W. Molecular spintronics using single-molecule magnets. *Nat. Mater.* **7**, 179-186 (2008).
3. Layfield, R.A. & Murugesu, M. Lanthanides and actinides in molecular magnetism. (John Wiley & Sons, 2015).

4. Ishikawa, N., Sugita, M., Ishikawa, T., Koshihara, S.-y. & Kaizu, Y. Lanthanide Double-Decker Complexes Functioning as Magnets at the Single-Molecular Level. *J. Am. Chem. Soc.* **125**, 8694-8695 (2003).
5. Thiele, S. et al. Electrically driven nuclear spin resonance in single-molecule magnets. *Science* **344**, 1135-1138 (2014).
6. Godfrin, C. et al. Operating Quantum States in Single Magnetic Molecules: Implementation of Grover's Quantum Algorithm. *Phys. Rev. Lett.* **119**, 187702 (2017).
7. Jiang, S.-D., Wang, B.-W., Sun, H.-L., Wang, Z.-M. & Gao, S. An Organometallic Single-Ion Magnet. *J. Am. Chem. Soc.* **133**, 4730-4733 (2011).
8. Rinehart, J.D. & Long, J.R. Exploiting single-ion anisotropy in the design of f-element single-molecule magnets. *Chem. Sci.* **2**, 2078-2085 (2011).
9. Guo, F.-S. et al. A Dysprosium Metallocene Single-Molecule Magnet Functioning at the Axial Limit. *Angew. Chem. Int. Ed.* **56**, 11445-11449 (2017).
10. Goodwin, C.A.P., Ortu, F., Reta, D., Chilton, N.F. & Mills, D.P. Molecular magnetic hysteresis at 60 kelvin in dysprosocenium. *Nature* **548**, 439-442 (2017).
11. Guo, F.-S. et al. Magnetic hysteresis up to 80 kelvin in a dysprosium metallocene single-molecule magnet. *Science* **362**, 1400 (2018).
12. Goodwin, C.A.P. et al. Terbocenium: completing a heavy lanthanide metallocenium cation family with an alternative anion abstraction strategy. *Chem. Commun.* **54**, 9182-9185 (2018).
13. Kotrle, K. & Herchel, R. Are Inorganic Single-Molecule Magnets a Possibility? A Theoretical Insight into Dysprosium Double-Deckers with Inorganic Ring Systems. *Inorg. Chem.* **58**, 14046-14057 (2019).
14. Wang, Y., Luo, Q.-C. & Zheng, Y.-Z. Organolanthanide Single-Molecule Magnets with Heterocyclic Ligands. *Angew. Chem. Int. Ed.* **63**, e202407016 (2024).
15. Evans, P., Reta, D., Whitehead, G.F.S., Chilton, N.F. & Mills, D.P. Bis-Monophospholyl Dysprosium Cation Showing Magnetic Hysteresis at 48 K. *J. Am. Chem. Soc.* **141**, 19935-19940 (2019).
16. Vanjak, J.C. et al. A High-Performance Single-Molecule Magnet Utilizing Dianionic Aminoborolide Ligands. *J. Am. Chem. Soc.* **144**, 17743-17747 (2022).
17. Vincent, A.H., Whyatt, Y.L., Chilton, N.F. & Long, J.R. Strong Axiality in a Dysprosium(III) Bis(borolide) Complex Leads to Magnetic Blocking at 65 K. *J. Am. Chem. Soc.* **145**, 1572-1579 (2023).
18. Dong, Z., Reinhold, C.R.W., Schmidtmann, M. & Müller, T. Trialkylsilyl-Substituted Silole and Germole Dianions. *Organometallics* **37**, 4736-4743 (2018).
19. Sun, X., Münzfeld, L., Jin, D., Hauser, A. & Roesky, P.W. Silole and germole complexes of lanthanum and cerium. *Chem. Commun.* **58**, 7976-7979 (2022).
20. Sun, X. & Roesky, P.W. Group 14 metallole dianions as η5-coordinating ligands. *Inorg. Chem. Front.* **10**, 5509-5516 (2023).
21. De, S., Mondal, A., Giblin, S.R. & Layfield, R.A. Bimetallic Synergy Enables Silole Insertion into THF and the Synthesis of Erbium Single-Molecule Magnets. *Angew. Chem. Int. Ed.* **63**, e202317678 (2024).
22. Tholen, P., Dong, Z., Schmidtmann, M., Albers, L. & Müller, T. A Neutral η5-Aminoborole Complex of Germanium(II). *Angew. Chem. Int. Ed.* **57**, 13319-13324 (2018).
23. Dong, Z., Janka, O., Kösters, J., Schmidtmann, M. & Müller, T. A Dimeric η1,η5-Germole Dianion Bridged Titanium(III) Complex with a Multicenter Ti–Ge–Ge–Ti Bond. *Angew. Chem. Int. Ed.* **57**, 8634-8638 (2018).
24. Dong, Z., Albers, L., Schmidtmann, M. & Müller, T. A Germacalicene: Synthesis, Structure, and Reactivity. *Chem. Eur. J.* **25**, 1098-1105 (2019).
25. Dong, Z., Albers, L. & Müller, T. Trialkylsilyl-Substituted Silole and Germole Dianions as Precursors for Unusual Silicon and Germanium Compounds. *Acc. Chem. Res.* **53**, 532-543 (2020).
26. Liu, J. et al. Yttrium germole dianion complexes with Y–Ge bonds. *Dalton Trans.* **50**, 5552-5556 (2021).

27. De, S., Mondal, A., Ruan, Z.-Y., Tong, M.-L. & Layfield, R.A. Dynamic Magnetic Properties of Germole-ligated Lanthanide Sandwich Complexes. *Chem. Eur. J.* **n/a**, e202300567 (2023).
28. Kuwabara, T. et al. Synthesis, Structures, and Electronic Properties of Triple- and Double-Decker Ruthenocenes Incorporated by a Group 14 Metallole Dianion Ligand. *J. Am. Chem. Soc.* **136**, 13059-13064 (2014).
29. Saito, M. et al. Dilithioplumbole: A Lead-Bearing Aromatic Cyclopentadienyl Analog. *Science* **328**, 339-342 (2010).
30. Saito, M. et al. Inverted Sandwich Rh Complex Bearing a Plumbole Ligand and Its Catalytic Activity. *Organometallics* **38**, 3099-3103 (2019).
31. Münzfeld, L. et al. Introduction of plumbole to f-element chemistry. *Chem. Sci.* **13**, 945-954 (2022).
32. Sun, X. et al. Triple-decker complexes incorporating three distinct deck architectures. *Chem. Commun.* **58**, 673-676 (2022).
33. Diaz-Rodriguez, R.M., Kitos, A.A. & Murugesu, M. Expanding the series of alkali metal plumbolyl complexes to Na and K. *Dalton Trans.* **51**, 14420-14428 (2022).
34. Saito, M., Haga, R., Yoshioka, M., Ishimura, K. & Nagase, S. The Aromaticity of the Stannole Dianion. *Angew. Chem. Int. Ed.* **44**, 6553-6556 (2005).
35. Masaichi, S. et al. Synthesis, Structure, and Reaction of Tetraethyldilithiostannole. *Chem. Lett.* **39**, 700-701 (2010).
36. Kuwabara, T., Saito, M., Guo, J.-D. & Nagase, S. Unexpected Formation of Ru2Sn2 Bicyclic Four-Membered Ring Complexes with Butterfly and Inverse-Sandwich Structures. *Inorg. Chem.* **52**, 3585-3587 (2013).
37. Kuwabara, T. & Saito, M. Synthesis of a Stannole Dianion Complex Bearing a μ-η1;η1-Coordination Mode: Different Electronic State of Stannole Dianion Ligands Depending on Their Hapticity. *Organometallics* **34**, 4202-4204 (2015).
38. Saito, M. et al. Heterobimetallic triple-decker complexes derived from a dianionic aromatic stannole ligand. *Dalton Trans.* **47**, 8892-8896 (2018).
39. Saito, M. et al. Anionic Stannaferrocene and Its Unique Electronic State. *Chem. Lett.* **48**, 163-165 (2019).
40. De, S., Mondal, A., Chen, Y.-C., Tong, M.-L. & Layfield, R.A. Single-molecule Magnet Properties of Silole- and Stannole-ligated Erbium Cyclo-octatetraenyl Sandwich Complexes. *Chem. Eur. J.* **n/a**, e202500011.
41. Kuwabara, T. et al. Enhancement of Stannylene Character in Stannole Dianion Equivalents Evidenced by NMR and Mössbauer Spectroscopy and Theoretical Studies of Newly Synthesized Silyl-Substituted Dilithiostannoles. *Organometallics* **33**, 2910-2913 (2014).
42. Gould, C.A. et al. Synthesis and Magnetism of Neutral, Linear Metallocene Complexes of Terbium(II) and Dysprosium(II). *J. Am. Chem. Soc.* **141**, 12967-12973 (2019).
43. McClain, R.K. et al. High-temperature magnetic blocking and magneto-structural correlations in a series of dysprosium(iii) metallocenium single-molecule magnets. *Chem. Sci.* **9**, 8492-8503 (2018).
44. Hauser, A. et al. Cycloheptatrienyl-Bridged Triple-Decker Complexes. *J. Am. Chem. Soc.* **146**, 13760-13769 (2024).
45. Woodruff, D.N., Winpenny, R.E.P. & Layfield, R.A. Lanthanide Single-Molecule Magnets. *Chem. Rev.* **113**, 5110-5148 (2013).
46. Blackmore, W.J.A. et al. Characterisation of magnetic relaxation on extremely long timescales. *PCCP* **25**, 16735-16744 (2023).
47. Aquilante, F. et al. Molcas 8: New capabilities for multiconfigurational quantum chemical calculations across the periodic table. *J. Comput. Chem.* **37**, 506-541 (2016).
48. Gould, C.A. et al. Ultrahard magnetism from mixed-valence dilanthanide complexes with metal-metal bonding. *Science* **375**, 198-202 (2022).
49. Meyer, G. & Ax, P. An analysis of the ammonium chloride route to anhydrous rare-earth metal chlorides. *Mater. Res. Bull.* **17**, 1447-1455 (1982).

Acknowledgements

S.S. and M.R. gratefully acknowledge support from the Deutsche Forschungsgemeinschaft (DFG, German Research Foundation) through the Collaborative Research Centre "4f for Future" (CRC 1573, project no. 471424360, project B2). Deutsche Forschungsgemeinschaft (DFG) is acknowledged for financial support within the Reinhart Koselleck-Projekt 440644676, RO 2008/19-1.

General procedures

All air- and moisture-sensitive manipulations were performed under dry N_2 or Ar atmosphere using standard Schlenk techniques or in an argon-filled MBraun glovebox, unless otherwise stated. *n*-Pentane and toluene were dried using an MBraun solvent purification system (SPS-800) and degassed. THF was distilled under nitrogen from potassium benzophenone ketyl. THF-d_8 was dried over Na-K alloy and degassed by freeze-pump-thaw cycles. 1,1,3,4-Tetraphenyl-2,5-bis(tert-butyldimethylsilyl)stannole[41] was prepared according to the literature procedures and DyI_3 was synthesized using a analogues route as the synthesis for the rare-earth trichlorides.[49] All other chemicals were obtained from commercial sources and used without further purification. Elemental analyses were carried out with an Elementar vario MICRO cube. NMR spectra were recorded on Bruker spectrometers (Avance Neo 300 MHz, Avance Neo 400 MHz or Avance III 400 MHz). Chemical shifts are referenced internally using signals of the residual protio solvent (^{1}H) or the solvent (^{13}C{^{1}H} and are reported relative to tetramethylsilane (^{1}H, ^{13}C{^{1}H}), or externally relative to tetramethylsilane (^{29}Si), tetramethyltin (^{119}Sn). All NMR spectra were measured at 298 K, unless otherwise specified. The multiplicity of the signals is indicated as s = singlet, d = doublet, dd = doublet of doublets, t = triplet, q = quartet, m = multiplet and br = broad. Assignments were determined based on unambiguous chemical shifts, coupling patterns and ^{13}C-DEPT experiments or 2D correlations (^{1}H-^{1}H COSY, ^{1}H-^{13}C HMQC and ^{1}H-^{13}C HMBC). Infrared (IR) spectra were recorded in the region 4000–400 cm^{-1} on a Bruker Tensor 37 FTIR spectrometer equipped with a room temperature DLaTGS detector, a diamond attenuated total reflection (ATR) unit and a nitrogen-flushed chamber. In terms of their intensity, the signals were classified into different categories (vs = very strong, s = strong, m = medium, w = weak, and sh = shoulder). All experimental magnetometry was carried out on polycrystalline samples of the respective compounds. The samples were placed in a glass tube alongside eicosane using a glovebox. Outside of the glovebox, using standard Schlenk techniques, the samples were flame sealed in the glass tubes and the eico was gently melted at 40 °C to prevent sample movement. Temperature dependent susceptibility data was collected in a range of 300 K – 2 K using a Quantum Design MPMS 3 SQUID magnetometer either upon cooling or upon heating after cooling the sample to 2 K at zero field or 1000 Oe. The external field during the measurement was 1000 Oe. All data were corrected for diamagnetic contributions of the sample holder and eicosane based on reference measurements and for the samples' intrinsic diamagnetism using Pascal's constants. Field dependent magnetization data was collected in a maximum range of -7 T to 7 K using a Quantum Design MPMS 3 SQUID magnetometer. Single quadrant M(H) curves were obtained using the "stable at each field" mode, while hysteresis measurements were performed in "continuous sweep" mode with a sweep rate of 50 Oe/s. Due to its long relaxation time at low *T*, the relaxation times for 2-Dy below 30 K were determined using magnetization decay data. The measurements were performed on a Quantum Design MPMS 3 SQUID magnetometer by increasing the field to the maximum of 7 T and a waiting step of 10 min to magnetically saturate the sample. The field was then switched off as fast as possible (700 Oe/s, linear mode) and the magnetization was

recorded during this whole procedure. Alternating current (AC) susceptibility data were recorded on a Quantum Design MPMS XL SQUID magnetometer in the frequency window of 0.1 Hz – 1500 Hz. Measurements have been performed either with or without an additional external DC field, for every data set the DC field is given. The amplitude of the alternating field was 5 Oe. For 2-Dy ab inito CASSCF/RASSI/SINGLE_ANISO calculations were performed using OpenMolcas.[47] The input structure was taken from the x-ray crystallographic structure refinement without further optimization. All basis sets were taken from the internal ANO-RCC library and the size of the basis sets was assigned as follows: VTZP (for Dy), VDZP (for Sn, K, O and the 8 C's of the stannole rings), VDZ (all others). The CASSCF were performed individually including the highest possible number of CI roots (21, 224 and 490 for sextet, quartet and doublet respectively) and of those 21, 128 and 130 were employed in the RASSI routine.

Synthesis of complex 1

To 1,1,3,4-tetraphenyl-2,5-bis(tert-butyldimethylsilyl)stannole (0.700 g, 0.992 mmol) and potassium chunk (0.660 g, 16.8 mmol) placed in a Young Schlenk flask, Et_2O (*ca.* 10 mL) was condensed at -88 °C. The solution was allowed to warm up to room temperature and stirred for 10 min. After freeze-pump-thaw cycles, the mixture was heated 75 °C for 72 h. The deep red suspension was cooled down to room temperature, extracted with 60 ml Et_2O to remove unreacted potassium and insoluble materials. After removal of the solvent, the red solid was washed with 20 ml of *n*-pentane to give the crude product, which is analytically pure and can be used for further reactions without further purification steps. Yield: 0.450 g, 69%. (Calculated with 0.45 coordinated Et_2O, as proven by NMR spectroscopy and elemental analysis). ^{1}H NMR (400.3 MHz, THF-d_8): δ (ppm) = 6.78-6.74 (m, 8H, H_{Ph}), 6.68-6.65 (m, 2H, H_{Ph}), 3.38 (q, ^1J = 7.0 Hz, CH_2 (Et_2O)), 1.12 (t, ^1J = 7.0 Hz, CH_3 (Et_2O)), .0.99 (s, 18H, Si*t*BuMe_2), –0.16 (s, 12H, Si*t*BuMe_2). ^{13}C{^{1}H} NMR (100.67 MHz, THF-d_8): δ (ppm) = 176.1 ($C_{\square}$), 155.8 ($C_{\square}$), 145.9 (C_{Ph}, q), 132.0 (C_{Ph}), 126.6 (C_{Ph}), 122.5 (C_{Ph}), 66.7 (CH_2, Et_2O), 30.6 (Si*t*BuMe$_2$), 19.1 (Si*t*BuMe$_2$), 16.1 (CH_3, Et_2O), 4.1 (Si*t*BuMe_2). ^{29}Si{^{1}H} NMR (79.52 MHz, THF-d_8): δ (ppm) = -5.9. ^{119}Sn NMR (101.0 MHz, THF-d_8): δ (ppm) = 615.5. Anal. Calcd for $C_{28}H_{49}K_2Si_2Sn$·0.45 (Et_2O) (663.06): C 53.98; H 6.76. Found: C 53.86, H 6.29. IR (ATR): $\tilde{\nu}$ (cm^{-1}) = 412 (vw), 448 (w), 494 (w), 559 (w), 594 (m), 633 (m), 653 (m), 698 (s), 762 (s), 797 (s), 815 (s), 952 (s), 1003 (w), 1022 (w), 1071 (m), 1098 (w), 1139 (w), 1153 (w), 1178 (w), 1196 (m), 1237 (s), 1329 (m), 1382 (m), 1403 (w), 1438 (m), 1466 (m), 1487 (m), 1587 (m), 2845 (vs), 2881 (s), 2922 (vs), 2943 (vs), 3014 (w), 3051 (w), 3068 (w).

Synthesis of complex 2-Tb

The dipotassium stannole **1** (0.144 g, 0.217 mmol) and anhydrous TbI_3 (0.058 g, 0.108 mmol) were placed together in a J. Young Schlenk flask. THF (ca. 5 mL) was condensed to the flask at -88 °C and the solution was allowed to warm up to room temperature and stirred for 16 h at room temperature. During this time, colorless insoluble materials (KI) formed. After filtration, the solution was concentrated to ca. 2 mL and layered with *n*-pentane. After two weeks, block-shaped dark red crystals formed. The solution was carefully decanted and the crystals were isolated. Crystalline yield: 0.088 g, 54%. Anal. Calcd for $C_{56}H_{80}TbKSi_4Sn_2$·3 (C_4H_8O) (1517.36): C 53.83; H 6.91. Found: C 54.34, H 6.94. IR (ATR): $\tilde{\nu}$ (cm^{-1}) = 386 (s), 395 (s), 447 (s), 472 (m), 486 (s), 515 (m), 532 (m), 539 (m), 564 (m), 590 (m), 622 (m), 629 (m), 659 (s), 676 (m), 699 (vs), 729 (m), 764 (vs), 804 (vs), 821 (s), 863 (w), 875 (w), 913 (w), 955 (m), 982 (w), 1005 (m), 1021 (w), 1050 (w), 1069 (w), 1154 (w), 1182 (w), 1191 (m), 1243(s), 1313

(w), 1331 (w), 1357 (w), 1385 (w), 1405 (w), 1439 (w), 1461 (m), 1469 (m), 1488 (w), 1593 (w), 2849 (m), 2880 (m), 2923 (m), 2948 (m), 3053 (vw).

Synthesis of complex 2-Dy

The dipotassium stannole 1 (0.120 g, 0.180 mmol) and anhydrous DyI_3 (0.049 g, 0.090 mmol) were placed together in a J. Young Schlenk flask. THF (ca. 5 mL) was condensed to the flask at -88 °C and the solution was allowed to warm up to room temperature and stirred for 16 h at room temperature. During this time, colorless insoluble materials (KI) formed. After filtration, the solution was concentrated to ca. 2 mL and layered with *n*-pentane. After two weeks, block-shaped dark red crystals formed. The solution was carefully decanted and the crystals were isolated. Crystalline yield: 0.064 g, 47%. Anal. Calcd for $C_{56}H_{80}DyKSi_4Sn_2 \cdot 3\,(C_4H_8O)$ (1520.94): C 53.70; H 6.89. Found: C 53.53; H 6.58. IR (ATR): $\tilde{\nu}$ (cm^{-1}) = 408 (vw), 448 (vw), 485 (w), 567 (w), 575 (w), 590 (w), 625 (w), 657 (m), 676 (m), 690 (m), 704 (m), 764 (s), 797 (s), 821 (s), 864 (w), 895 (w), 913 (w), 956 (m), 1003 (w), 1024 (w), 1053 (m), 1069 (w), 1155 (w), 1190 (m), 1241 (s), 1317 (w), 1356 (w), 1384 (w), 1405 (w), 1440 (m), 1466 (m), 1489 (m), 1573 (w), 1593 (w), 2697 (w), 2847 (vs), 2875 (s), 2920 (vs), 2947 (s), 3053 (w).

Synthesis of complex 3-Tb

Complex **2-Tb** (0.051 g, 0.033 mmol and 18-crown-6 (0.018 g, 0.068 mmol were placed together in a J. Young Schlenk flask. THF (ca. 2 mL) was added to the flask and the solution was removed under reduced pressure until only tiny amount of THF is left. ca. 3 mL of benzene was added to the flask. After one day, red crystals were formed. Crystalline yield: 0.023 g, 38%. Anal. Calcd for $C_{74}H_{116}TbKO_9Si_4Sn_2 \cdot 2(C_6H_6)$ (1853.74): C 55.72; H 6.96. Found: C 55.83, H 6.70. IR (ATR): $\tilde{\nu}$ (cm^{-1}) = 386 (m), 395 (m), 408 (m), 434 (w), 447 (w), 472 (w), 492 (m), 530 (m), 567 (m), 591 (m), 622 (w), 629 (w), 656 (m), 678 (m), 699 (s), 765 (s), 804 (s), 822 (s), 855 (m), 863 (m), 945 (s), 957 (s), 985 (m), 1005 (m), 1022 (m), 1072 (m), 1106 (vs), 1185 (w), 1243 (s), 1286 (w), 1297 (w), 1352 (m), 1384 (w), 1442 (w), 1469 (m), 1488 (w), 1593 (w), 2848 (m), 2917 (m), 2946 (m), 3049 (vw).

Synthesis of complex 4-Dy

Complex **2-Dy** (0.050 g, 0.033 mmol and 18-crown-6 (0.019 g, 0.072 mmol were placed together in a J. Young Schlenk flask. THF (ca. 2 mL) was added to the flask and the solution was concentrated and layered with benzene. After three days, red crystals were formed. Crystalline yield: 0.025 g, 33%. Anal. Calcd. for $C_{96}H_{160}DyKO_{16}Si_4Sn_2 \cdot 2(C_6H_6)$ (2317.00): C 55.99; H 7.48. Found: C 56.06, H 7.23. IR (ATR): $\tilde{\nu}$ (cm^{-1}) = 378 (m), 387 (m), 404 (m), 447 (m), 466 (w), 485 (m), 502 (w), 513 (w), 530 (m), 542 (w), 556 (m), 567 (m), 591 (m), 621 (m), 628 (m), 653 (m), 669 (m), 699 (s), 730 (m), 760 (s), 802 (s), 819 (s), 860 (w), 909 (w), 945 (m), 960 (s), 1006 (w), 1022 (w), 1055 (m), 1069 (m), 1103 (vs), 1182 (w), 1236 (m), 1284 (w), 1351 (m), 1381 (w), 1437 (w), 1454 (w), 1469 (w), 1488 (w), 1590 (w), 2690 (vw), 2838 (m), 2885 (m), 2913 (m), 2944 (w), 3045 (vw).

Data availability

All synthetic protocols, spectroscopic data (NMR, IR), detailed crystallographic information, quantum chemical calculations, magnetic measurements, and CASSCF Calculations can be found in the Supplementary Information. Data for this paper are available at radar4chem doi:10.22000/gbqsqjy6hbdxjsz8. Crystallographic data for the structures reported in this Article have been deposited at the Cambridge Crystallographic Data Centre, under deposition numbers

CCDC 2429603 (**1**), 2429604 (**2-Dy**), 2429605 (**2-Tb**), 2429606 (**3**), 2429607 (**4**)**.** Copies of the data can be obtained free of charge via https://www.ccdc.cam.ac.uk/structures/.

Author contributions

X.S. synthesized all the compounds described, determined and interpreted the X-ray structures, conducted NMR experiments. A.H. repeated the syntheses of all compounds. D.J. and S.M. contributed to analyses. S.S. performed SQUID measurements and analysed the data. M.S. advised on experiments. The project was directed by M.R. and P.W.R. P.W.R. initiated the project.

Competing Interests Statement

We declare that none of the authors have competing financial or non-financial interests as defined by Nature Portfolio.